

Article

## Complexes in the Photocatalytic Reaction of CO<sub>2</sub> and H<sub>2</sub>O: Theoretical Studies

Dongmei Luo <sup>1,2</sup>, Ning Zhang <sup>1,\*</sup>, Sanguo Hong <sup>1</sup>, Huanwen Wu <sup>1</sup> and Zhihua Liu <sup>1</sup>

<sup>1</sup> Department of Chemistry, Nanchang University, Nanchang 330031, China;  
E-Mails: luodongmei1976@yahoo.com.cn (D.L.); sanguohong@jxedu.gov.cn (S.H.);  
wuhuanwen123@126.com (H.W.); lzh851104@yahoo.com.cn (Z.L.)

<sup>2</sup> Department of Chemistry, Qiqihaer University, Qiqihaer 161006, China

\* Author to whom correspondence should be addressed; E-Mail: nzhang.ncu@163.com;  
Tel.: +86-791-3969-332; Fax: +86-791-3969-338.

Received: 5 July 2010; in revised form: 16 July 2010 / Accepted: 18 July 2010 /

Published: 29 July 2010

---

**Abstract:** Complexes (H<sub>2</sub>O/CO<sub>2</sub>, e<sup>-</sup>(H<sub>2</sub>O/CO<sub>2</sub>) and h<sup>+</sup>-(H<sub>2</sub>O/CO<sub>2</sub>)) in the reaction system of CO<sub>2</sub> photoreduction with H<sub>2</sub>O were researched by B3LYP and MP2 methods along with natural bond orbital (NBO) analysis. Geometries of these complexes were optimized and frequencies analysis performed. H<sub>2</sub>O/CO<sub>2</sub> captured photo-induced electron and hole produced e<sup>-</sup>(H<sub>2</sub>O/CO<sub>2</sub>) and h<sup>+</sup>-(H<sub>2</sub>O/CO<sub>2</sub>), respectively. The results revealed that CO<sub>2</sub> and H<sub>2</sub>O molecules could be activated by the photo-induced electrons and holes, and each of these complexes possessed two isomers. Due to the effect of photo-induced electrons, the bond length of C=O and H-O were lengthened, while H-O bonds were shortened, influenced by holes. The infrared (IR) adsorption frequencies of these complexes were different from that of CO<sub>2</sub> and H<sub>2</sub>O, which might be attributed to the synergistic effect and which could not be captured experimentally.

**Keywords:** e<sup>-</sup>(H<sub>2</sub>O/CO<sub>2</sub>); h<sup>+</sup>-(H<sub>2</sub>O/CO<sub>2</sub>); photocatalytic reaction; theoretical studies

---

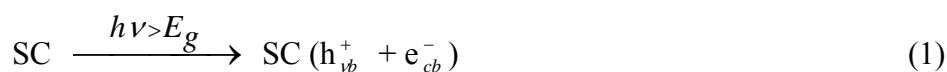
## 1. Introduction

Greenhouse gas CO<sub>2</sub> is the primary cause of global warming. The transformation from CO<sub>2</sub> to fuel-like hydrocarbon is becoming one of the most important areas of chemical research, which is not only for solving the urgent greenhouse effect, but also for finding a new approach to obtain energy.

As the Earth's ultimate power supply and an environmentally friendly energy source [1–5], light can activate reactants and promote a reaction. While the reduction of CO<sub>2</sub> with H<sub>2</sub>O is very difficult with thermal surface catalysis, photo stimulating surface catalysis is of great theoretical and practical value. Many researches [6] have shown that CO<sub>2</sub> could be reduced by water vapor or solvent with photocatalysts. Among these photocatalysts, TiO<sub>2</sub> or modified TiO<sub>2</sub> may promote the photoreduction of CO<sub>2</sub> to useful organic compounds [7–13], such as formate, carbon monoxide, methane and ethanol. The optical and electronic properties of nanostructured TiO<sub>2</sub> can be adjusted by thermal treatments [14], supported film growth [15], and metal-ion doping [16].

During our research on the reaction of H<sub>2</sub>O and CO<sub>2</sub> over photocatalysts, we found methanol as a product [17], which meant that there must be some advantageous factors for forming C–H bond in the reaction. The photocatalytic production of CH<sub>4</sub> from CO<sub>2</sub> and H<sub>2</sub>O on Pt/SrTiO<sub>3</sub> catalysts has also been reported by Hemminger *et al.* [18].

H<sub>2</sub>O may reduce CO<sub>2</sub> to CH<sub>4</sub>, CH<sub>3</sub>OH, and CO over the anchored titanium oxide catalysts at 323 K under UV irradiation [19]. A reaction scheme is proposed for the photocatalytic reduction of CO<sub>2</sub> with H<sub>2</sub>O as follows: TiO<sub>2</sub>  $\xrightarrow{h\nu}$  e<sup>-</sup><sub>cb</sub>(TiO<sub>2</sub>) + h<sup>+</sup><sub>vb</sub>(TiO<sub>2</sub>). Incident photons are absorbed by TiO<sub>2</sub>, and photo-excited electrons (e<sup>-</sup>) and positive holes (h<sup>+</sup>) are produced in the catalyst by charge transfer to the excited state of (Ti<sup>3+</sup>–O<sup>-</sup>)\*. Furthermore, the photo-excited electrons and holes in the lattice are separated and trapped by appropriate sites of TiO<sub>2</sub> to avoid recombination. The interaction of CO<sub>2</sub> molecules with the excited state of (Ti<sup>3+</sup>–O<sup>-</sup>)\* leads to the formation of CO<sub>2</sub><sup>-•</sup> radicals [5]. The semiconductor (SC) bandgap excitation leads to the formation of conduction band electrons and valance band holes, which serve as the sites for photoreduction and photooxidation, respectively [13]. The photo-oxidation of H<sub>2</sub>O led to the formation of hydroxyl radicals OH and H<sup>+</sup> [14].



The hydroxyl radicals generate oxygen while H<sup>+</sup> ions form hydrogen by capturing conduction band electrons [15,16,18].

Photocatalytic reaction is the interaction between photo-induced electrons and holes on the photocatalyst surface with reactants. In order to know the details of the interaction among the reactants, the photo-induced electrons and holes, and the situation of activated reactants, which were referenced by Inokuchi Y. *et al.* [20], we calculated the interaction between photo-induced electrons and holes with H<sub>2</sub>O/CO<sub>2</sub> as complexes. There are few reports on such complexes.

## 2. Computational Details

The geometries of  $\text{H}_2\text{O}$ ,  $\text{CO}_2$ ,  $\text{CO}_2^{\bullet-}$ ,  $\text{H}_2\text{O}^+$ ,  $\text{H}_2\text{O}/\text{CO}_2$ ,  $e^-(\text{H}_2\text{O}/\text{CO}_2)$  and  $h^+(\text{H}_2\text{O}/\text{CO}_2)$  were respectively optimized and then they were analyzed by natural bond orbital (NBO) [21] using density functional theory (DFT) (with correcting coefficient 0.96 of vibrational frequencies) [22–25] at the B3LYP [26–29] level and Møller–Plesset (MP2 (with correcting coefficient 0.92) ) perturbation theory [30] on different basis sets. Among these basis sets, 6–311 g\* [31,32] was employed in calculations as the optimal one. This work was carried out with the GAUSSIAN 03 program package [33].  $\text{CO}_2$  and  $\text{H}_2\text{O}$  were activated by photo-induced electrons and holes, which was confirmed by the change of geometry structure parameters and the charge distribution. NBO atomic charges and dipole moments of  $\text{CO}_2$  and  $\text{H}_2\text{O}$  are listed in Table 1, and the geometrical parameters are shown in Figure 1. All these data indicated great changes in the optimum geometrical parameters of  $\text{H}_2\text{O}/\text{CO}_2$ ,  $e^-(\text{H}_2\text{O}/\text{CO}_2)$  and  $h^+(\text{H}_2\text{O}/\text{CO}_2)$  complexes. The interaction energies when the photo-induced electrons and the holes were also taken into account. The thermochemical parameters of the system are shown in Table 2.

Herein,  $\text{H}_2\text{O}/\text{CO}_{2-1}$  refers to the complex of  $\text{CO}_2$  and  $\text{H}_2\text{O}$  combined by  $\text{O}\cdots\text{H}\cdots\text{O}$  (probable hydrogen bond between  $\text{CO}_2$  and  $\text{H}_2\text{O}$ , similarly hereinafter);  $\text{H}_2\text{O}/\text{CO}_{2-2}$ , complex of  $\text{CO}_2$  and  $\text{H}_2\text{O}$  combined by  $\text{C}\cdots\text{O}$  (probable bond between the carbon atom of  $\text{CO}_2$  and the oxygen atom of  $\text{H}_2\text{O}$ , similarly hereinafter);  $e^-\text{HC}_{-1}$ , the complex of  $\text{CO}_2$  and  $\text{H}_2\text{O}$  combined by  $\text{O}\cdots\text{H}\cdots\text{O}$  captured an electron;  $e^-\text{HC}_{-2}$ , the complex of  $\text{CO}_2$  and  $\text{H}_2\text{O}$  combined by  $\text{C}\cdots\text{O}$  captured an electron,  $h^+\text{HC}_{-1}$ , the complex of  $\text{CO}_2$  and  $\text{H}_2\text{O}$  combined by  $\text{O}\cdots\text{H}\cdots\text{O}$  captured a hole; ( $h^+\text{HC}_{-2}$ ), the complex of  $\text{CO}_2$  and  $\text{H}_2\text{O}$  combined by  $\text{C}\cdots\text{O}$  captured a hole.

## 3. Results and Discussion

### 3.1. Geometric Parameters Analysis

As shown in Figures 1 and 2, the geometrical parameters of all complexes revealed that bond lengths and bond angles were almost the same in  $\text{H}_2\text{O}/\text{CO}_{2-1}$  and  $\text{H}_2\text{O}/\text{CO}_{2-2}$ . According to both B3LYP and MP2 method, the total dipole moments of  $\text{H}_2\text{O}/\text{CO}_2$  was a little greater than that of  $\text{H}_2\text{O}$ , indicating that the complex  $\text{H}_2\text{O}/\text{CO}_2$  could not obviously change the properties of  $\text{H}_2\text{O}$  and  $\text{CO}_2$  molecules.

**Figure 1.** Optimized geometry structure and total NBO charge distribution of the complexes by B3LYP.

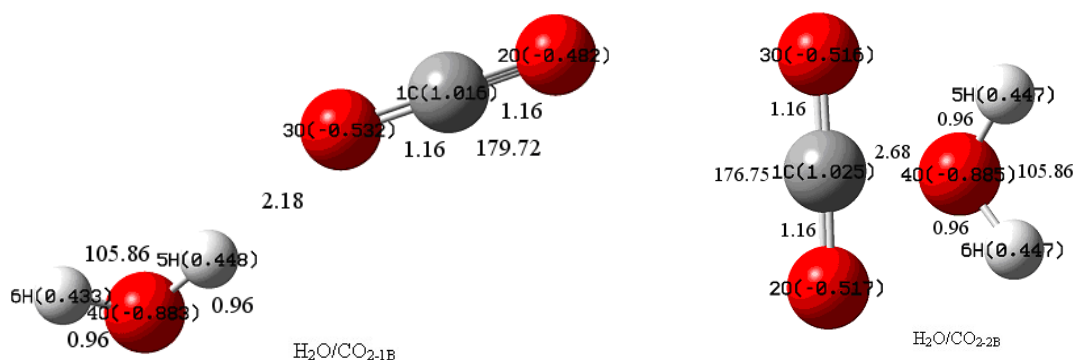
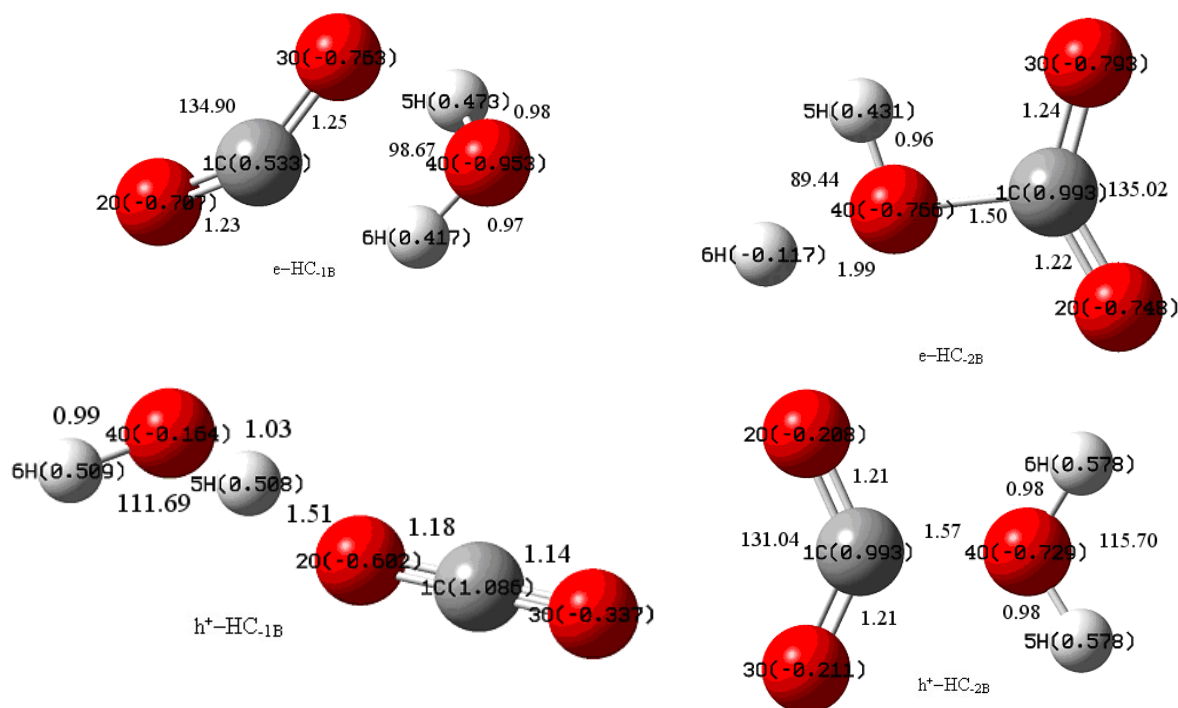
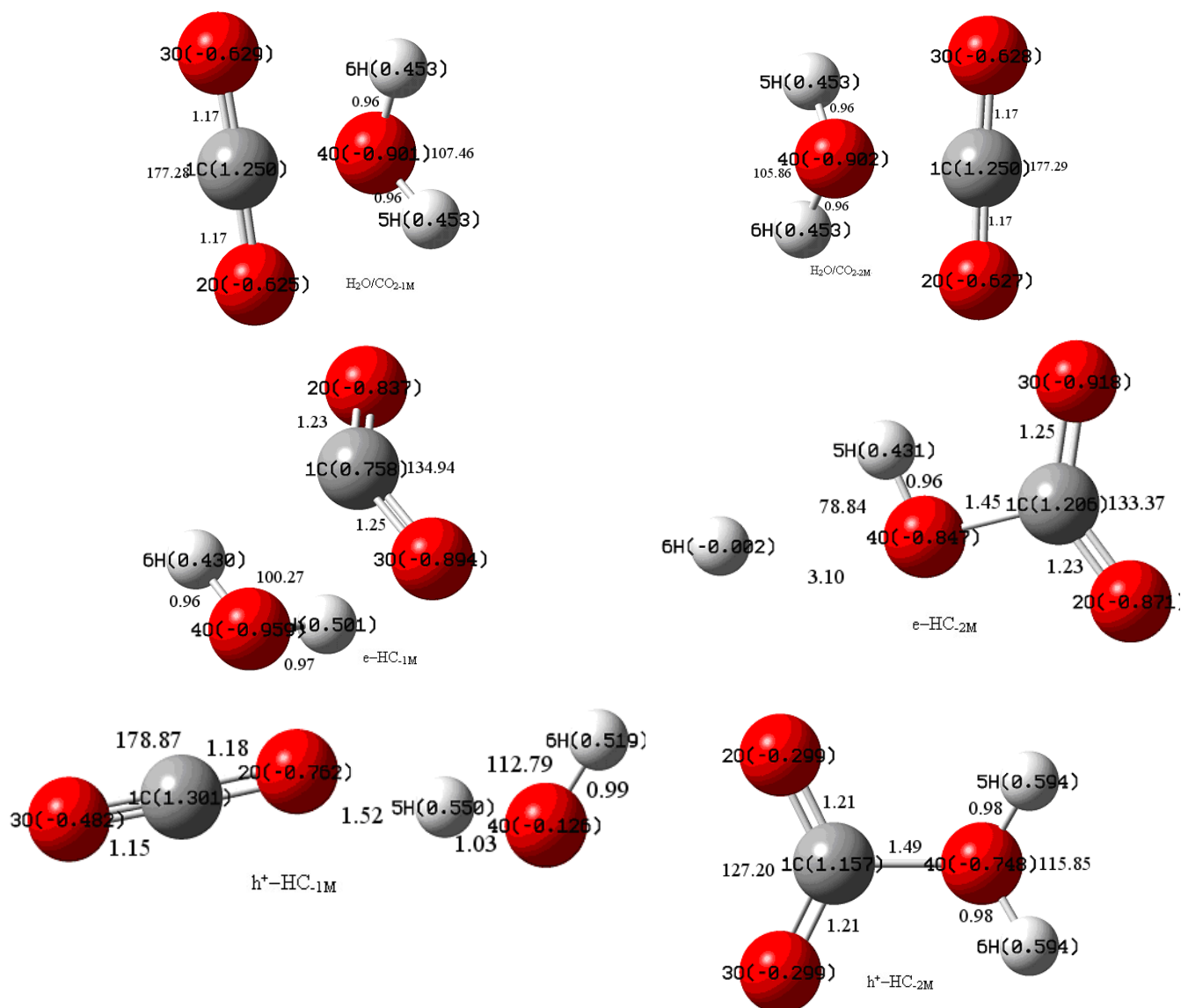


Figure 1. Cont.



Calculated structural parameters of  $e\text{-HC}_1$  and  $e\text{-HC}_2$  by B3LYP were different from that of  $\text{CO}_2$  and  $\text{H}_2\text{O}$ . The C=O bond was lengthened by 0.06–0.09 Å compared to that in  $\text{CO}_2$  while approximately equal to that in  $\text{CO}_2^*$ , and the length of H–O bond was also lengthened by 0.01–0.02 Å compared to that in  $\text{H}_2\text{O}$  while it was shorter than that in  $\text{H}_2\text{O}^+$ . Therefore,  $\text{CO}_2$  was activated and the repulsion force between C and O was strengthened. The bond angle  $A_{\text{H-O-H}}$  was reduced by 7–17 degrees compared to that in  $\text{H}_2\text{O}/\text{CO}_2$ , while the bond length of H–O was 3.10 Å by MP2, which indicated the dissociation of the bond. The bond length of ( $\text{CO}_2$ )  $\text{O}\cdots\text{H}$  was 1.89 Å, which was close to that of hydrogen bond. The photo-induced electron in  $e\text{-HC}_1$  enhanced the activation of  $\text{CO}_2$  and  $\text{H}_2\text{O}$ . In  $e\text{-HC}_2$ , the bond length of ( $\text{H}_2\text{O}$ )  $\text{O}\cdots\text{C}$  was 1.50 Å by B3LYP and 1.45 Å by MP2, which was close to the length of C–O bond. One of the H atoms of  $\text{H}_2\text{O}$  was dissociated from the original bonding O atom. In  $h^+\text{-HC}_1$ , it was shown by B3LYP that one C–O bond length was shortened by 0.02 Å compared to that of  $\text{CO}_2$  and the other was lengthened 0.02 Å. The short one was near the triple bond, which might lead to CO formation. At the same time the O atom of  $\text{CO}_2$  may form a hydrogen bond with a length of 1.51 Å. The corresponding O–H bond was lengthened 0.07 Å. In  $h^+\text{-HC}_2$ , both C–O bonds were lengthened 0.05 Å,  $\text{C}\cdots\text{O}$  ( $\text{H}_2\text{O}$ ) bond length was 1.57 Å, while both H–O bonds were lengthened 0.02 Å, and the bond angle of O–H–O was increased by about 6–10 degrees. On the other hand, by MP2, the calculated structural parameters of  $h^+\text{-HC}_2$  were much different than from B3LYP, which indicated that the  $h^+\text{-HC}_1$  complex was not as stable as  $h^+\text{-HC}_2$ . This was consistent with the following thermochemistry data. The dipole moments of both  $h^+\text{-HC}_1$  and  $h^+\text{-HC}_2$  were about three-times greater than that of  $\text{H}_2\text{O}/\text{CO}_{2-1}$  and  $\text{H}_2\text{O}/\text{CO}_{2-2}$  when calculated by B3LYP, and even greater when calculated by MP2, which indicated the breaking of symmetry in both  $h^+\text{-HC}_1$  and  $h^+\text{-HC}_2$ .

**Figure 2.** Optimized geometry structure and total NBO charge distribution of the complexes by MP2.



### 3.2. NBO Atomic Charge Analysis

The natural electron configuration of the complexes, as shown in Table 1, revealed the population of charges in H<sub>2</sub>O/CO<sub>2</sub>, which was different from that of H<sub>2</sub>O (O: 2s(1.75)2p(5.11)3d(0.01), H: 1s(0.56)) and CO<sub>2</sub> (C: 2s(0.64)2p(2.31)3p(0.03)3d(0.02); O: 2s(1.72)2p(4.76)3d(0.01)). This was evidence for the formation of a London dispersion complex [34]. The natural electron configuration of CO<sub>2</sub><sup>-</sup> and H<sub>2</sub>O<sup>+</sup> were shown as follows: the natural electron configuration of the C atom was 2s(0.97)2p(2.39)3s(0.06)3p(0.04)3d(0.01) and that of the O atom was 2s(1.74)2p(5.00) by B3LYP, while 2s(0.94)2p(2.20)3s(0.05)3p(0.04)3d(0.02) of the C atom and 2s(1.75)2p(5.12)3d(0.01) of the O atom by MP2 in CO<sub>2</sub><sup>-</sup>. The natural electron configuration of the O atom was 2s(1.81) 2p(4.26) and that of the H atom was 1s (0.46) by B3LYP, while 2s(1.79)2p(4.28)3d(0.01) of the O atom and 1s(0.46) of the H atom by MP2 in H<sub>2</sub>O<sup>+</sup>.

**Table 1.** Natural Electron Configuration of the complexes.

M	E	$h^+ - HC_{-1}$	$h^+ - HC_{-2}$	$e - HC_{-1}$	$e - HC_{-2}$	$H_2O/CO_{2-1}$	$H_2O/CO_{2-2}$
B	O	2s(1.69) g	2s(1.75)	2s(1.74)	2s(1.72)	2s(1.72)	2s(1.72)
3		2p(4.90) h	2p(4.45)	2p(4.96)	2p(5.02)	2p(4.75)	2p(4.78)
L		3d(0.01) i	3d(0.01)	3d(0.01)	3d(0.01)	3d(0.01)	3d(0.01)
Y	C	2s(0.62)	2s(0.68)	2s(0.96)	2s(0.67)	2s(0.64)	2s(0.64)
P		2p(2.25)	2p(2.27)	2p(2.40)	2p(2.27)	2p(2.30)	2p(2.29)
		3p(0.02)	3p(0.03)	3s(0.06)	3p(0.05)	3p(0.03)	3p(0.03)
		3d(0.02)	3d(0.02)	3p(0.04)	3d(0.02)	3d(0.02)	3d(0.02)
B				3d(0.01)			
3	O	2s(1.72)	2s(1.75)	2s(1.75)	2s(1.73)	2s(1.72)	2s(1.72)
L		2p(4.60)	2p(4.45)	2p(5.01)	2p(5.05)	2p(4.80)	2p(4.78)
Y		3d(0.01)	3d(0.01)	3d(0.01)	3d(0.01)	3d(0.01)	3d(0.01)
P	H	1s(0.49)	1s(0.42)	1s(0.52)	1s(0.56)	1s(0.55)	1s(0.55)
				2s(0.01)	2s(0.01)		
B	O	2s(1.79)	2s(1.65)	2s(1.75)	2s(1.75)	2s(1.75)	2s(1.75)
3		2p(4.37)	2p(5.07)	2p(5.19)	2p(5.00)	2p(5.13)	2p(5.13)
L		3d(0.01)		3d(0.01)		3d(0.01)	3d(0.01)
Y	H	1s(0.49)	1s(0.42)	1s(0.52)	1s(1.12)	1s(0.56)	1s(0.55)
P				2s(0.01)			
M	O	2s(1.70)	2s(1.75)	2s(1.74)	2s(1.73)	2s(1.72)	2s(1.72)
P		2p(5.05)	2p(4.54)	2p(5.08)	2p(5.13)	2p(4.89)	2p(4.89)
2				3p(0.01)			
		3d(0.01)	3d(0.01)	3d(0.01)	3d(0.01)	3d(0.01)	3d(0.01)
M	C	2s(0.63)	2s(0.66)	2s(0.93)	2s(0.66)	2s(0.65)	2s(0.65)
P		2p(2.02)	2p(2.11)	2p(2.20)	2p(2.06)	2p(2.05)	2p(2.05)
2		3p(0.02)	3p(0.03)	3s(0.05)	3p(0.04)	3p(0.03)	3p(0.03)
		3d(0.03)	3d(0.03)	3p(0.04)	3d(0.03)	3d(0.03)	3d(0.03)
M				3d(0.02)			
P	O	2s(1.72)	2s(1.75)	2s(1.75)	2s(1.74)	2s(1.72)	2s(1.72)
2		2p(4.75)	2p(4.54)	2p(5.13)	2p(5.17)	2p(4.89)	2p(4.89)
		3d(0.01)	3d(0.01)	3d(0.01)	3d(0.01)	3d(0.01)	3d(0.01)
M	H	1s(0.45)	1s(0.40)	1s(0.49)	1s(0.56)	1s(0.54)	1s(0.54)
P							
2	O	2s(1.78)	2s(1.64)	2s(1.75)	2s(1.73)	2s(1.74)	2s(1.74)
		2p(4.34)	2p(5.11)	2p(5.20)	2p(5.10)	2p(5.16)	2p(5.16)
M		3d(0.01)		3d(0.01)	3d(0.01)	3d(0.01)	3d(0.01)
P	H	1s(0.48)	1s(0.40)	1s(0.57)	1s(1.00)	1s(0.54)	1s(0.54)
2				2s(0.01)			

The population of charge in  $e-(H_2O/CO_2)$  was dispersed both by B3LYP and MP2. In  $e-HC_{-1}$ , there was 0.06 electrons on  $3s$  orbital of C atom, 0.04 electrons on  $3p$  orbital, and 0.01 electrons on  $3d$  orbital by B3LYP. In  $e-HC_{-2}$ ,  $3s$  orbital of C atom gained 0.00 electron, 0.05 (0.04 electrons by MP2) electron on  $3p$  orbital and 0.02 (0.03 electron by MP2) electrons on  $3d$  orbital by B3LYP. The contribution to the hybrid orbital from  $2s$  orbital and  $2p$  orbital were different in  $e-HC_{-1}$  and  $e-HC_{-2}$ .

The particular natural electron configuration of a H atom in  $e\text{-HC}_{.2}$  indicated that the H atom was a free radical which had 1.12 (1.00 electron by MP2) electrons on its  $1s$  orbital, and 0.01 electrons on the  $2s$  orbital of another H atom for the joining of the photo-induced electron by B3LYP.

The population of the charge in  $h^+(\text{H}_2\text{O}/\text{CO}_2)$  was dispersed. There was not so much difference in the charge distributions of  $h^+\text{-HC}_{.1}$  and  $h^+\text{-HC}_{.2}$  on the C atom and H atom by B3LYP, while the charge distribution of  $h^+\text{-HC}_{.2}$  was higher than that of  $h^+\text{-HC}_{.1}$  by MP2. The contribution of  $2p$  orbital in O atom of  $h^+\text{-HC}_{.1}$  and  $h^+\text{-HC}_{.2}$  to the hybrid orbital was different. As for  $\text{H}_2\text{O}/\text{CO}_{2.1}$  and  $\text{H}_2\text{O}/\text{CO}_{2.2}$ , the population of the charge was almost the same by both calculating methods.

The total NBO charge distribution of the complexes is presented in Figures 1 and 2. The positive charge on C was 0.460 electrons in  $e\text{-HC}_{.1}$ , which was lower than that in  $e\text{-HC}_{.2}$ . The O atom of  $\text{H}_2\text{O}$  in  $e\text{-HC}_{.1}$  obtained more negative charge than that of the others in both  $e\text{-HC}_{.1}$  and  $e\text{-HC}_{.2}$ . H atom was negatively charged for the effect of the photo-induced electron, where the corresponding values for the isolated  $\text{CO}_2^{\bullet-}$  and  $\text{H}_2\text{O}^+$  are shown as follows: 0.513  $e^-$  for C and -0.756  $e^-$  for O by B3LYP while 0.753  $e^-$  for C and -0.877  $e^-$  for O by MP2 in  $\text{CO}_2^{\bullet-}$ , -0.070  $e^-$  for O and 0.535  $e^-$  for H by B3LYP, and -0.082  $e^-$  for O and 0.541  $e^-$  for H by MP2 in  $\text{H}_2\text{O}^+$ . It is interesting that the charge of O atom from  $\text{H}_2\text{O}$  in  $h^+\text{-HC}_{.1}$  was different from that in  $h^+\text{-HC}_{.2}$  by both methods for different chemical environment around them. The unbalanced charge distribution of the two O atoms from  $\text{CO}_2$  in  $h^+\text{-HC}_{.1}$  was because of the tendency to form hydrogen bond. This phenomenon also existed in  $\text{H}_2\text{O}/\text{CO}_{2.2}$ .

The total NBO charge distribution in  $\text{H}_2\text{O}/\text{CO}_{2.2}$  was different from that of  $\text{H}_2\text{O}$  (O: -0.870  $e^-$ , H: 0.435  $e^-$ ),  $\text{CO}_2$  (C: 1.000  $e^-$ , O: -0.500  $e^-$ ) and  $\text{H}_2\text{O}/\text{CO}_{2.1}$  because of the interaction between C atom and O atom (from  $\text{H}_2\text{O}$ ). The greatest difference of the two calculating method is shown in  $e\text{-HC}_{.1}$  and  $e\text{-HC}_{.2}$ , especially for C and H atoms, while the tendency of the H dissociation was almost the same by B3LYP and MP2.

### 3.3. Thermochemistry Parameters Analysis

Thermochemistry parameters of the system are presented in Table 2. The interaction energies of  $\text{CO}_2$  and  $\text{H}_2\text{O}$  molecule including photo-induced electrons and corresponding holes were calculated using the following equations:

$$\Delta E_{HC} = E_{HC} - E_{\text{CO}_2} - E_{\text{H}_2\text{O}} \quad (3)$$

$$\Delta E_{e\text{-HC}} = E_{e\text{-HC}} - E_{\text{CO}_2^{\bullet-}} - E_{\text{H}_2\text{O}} \quad (4)$$

$$\Delta E_{h^+\text{HC}} = E_{h^+\text{HC}} - E_{\text{CO}_2} - E_{\text{H}_2\text{O}^+} \quad (5)$$

In the equation (1),  $\Delta E_{HC}$  could represent the calculated interaction energy values of the sum of electronic and thermal energies ( $E_{\text{tot}}$ ), the sum of electronic and thermal enthalpies (H) and the sum of electronic and thermal free energies (G) of  $\text{HC}_{.1}$  and  $\text{HC}_{.2}$ . In the equation (2)  $\Delta E_{e\text{-HC}}$  represents the same items of  $e\text{-HC}_{.1}$  and  $e\text{-HC}_{.2}$ , and then in the equation (3)  $\Delta E_{h^+\text{HC}}$  represents that of  $h^+\text{-HC}_{.1}$  and  $h^+\text{-HC}_{.2}$ . The corresponding entropy values were calculated by the following equation:

$$\Delta S = \frac{\Delta H - \Delta G}{T} \quad (6)$$

T refers to the reaction temperature of our experiment 333 K [17].

H<sub>2</sub>O/CO<sub>2-2</sub> had the maximum value of the entropy ( $\Delta S = -128.80$  J/mol·K) for its loose structure and poor symmetry. h<sup>+</sup>-HC<sub>-1</sub> had the highest energy ( $\Delta E_{\text{tot}} = -84.70$  KJ/mol) for the existence of dissociative H atom among the six complexes, while e-HC<sub>-2</sub> had the minimum entropy ( $\Delta S = -243.75$  J/mol·K) and the lowest energy ( $\Delta E_{\text{tot}} = 14.54$  kJ/mol) compared to the other five for its relatively stable skeletal structure as well as its good symmetry by B3LYP. This result was different from that by MP2, where HC<sub>-1</sub> and H<sub>2</sub>O/CO<sub>2-2</sub> had the maximum values of the entropy ( $\Delta S = -264.23$  J/mol·K) and h<sup>+</sup>-HC<sub>-1</sub> had the highest energy ( $\Delta E_{\text{tot}} = -77.75$  kJ/mol).

The enthalpy values of most of the six complexes were higher than that of the sum of CO<sub>2</sub> and H<sub>2</sub>O, the sum of CO<sub>2</sub> and H<sub>2</sub>O<sup>+</sup>, and the sum of H<sub>2</sub>O and CO<sub>2</sub><sup>•-</sup> for the forming of new bond and radicals. The Gibbs free energy values of most of the six complexes were lower than that of the sum of CO<sub>2</sub> and H<sub>2</sub>O, the sum of CO<sub>2</sub> and H<sub>2</sub>O<sup>+</sup>, and the sum of H<sub>2</sub>O and CO<sub>2</sub><sup>•-</sup>, where the necessary energy for photo-induced electrons and holes to charge the reactants from the environment of the photoreaction system is available. It is interesting that the highest  $\Delta G$  was in h<sup>+</sup>-HC<sub>-2</sub>, which indicated the instability of h<sup>+</sup>-HC<sub>-1</sub>. This was consistent with the structural parameters at the same level. No thermochemistry experimental data now for these complexes were available for the complicated photocatalytic reaction environment. Counterpoise calculations at the B3LYP/6-311G\*\*//6-311++G\*\* level and the MP2/6-311G\*\*//6-311++G\*\* level suggested that basis set superposition errors (BSSE) were nearly the same (2.09 kJ/mol) for all conformers. Since it is not clear that such corrections improved the reliability of the results [35–40], we did not included them in Table 2.

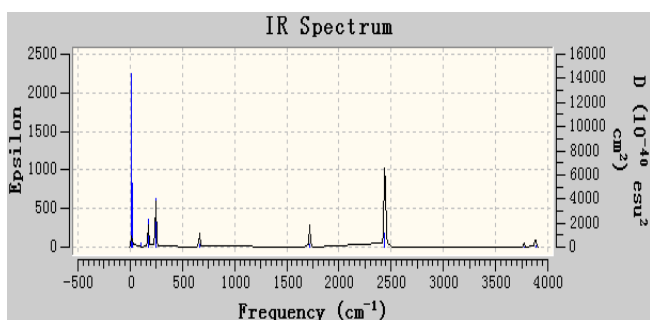
**Table 2.** Thermochemistry Parameters of Complexes.

Method parameter	B3LYP				MP2			
	$\Delta E_{\text{tot}}$ kJ/mol	$\Delta H$ kJ/mol	$\Delta G$ kJ/mol	$\Delta S$ J/mol·K	$\Delta E_{\text{tot}}$ kJ/mol	$\Delta H$ kJ/mol	$\Delta G$ kJ/mol	$\Delta S$ J/mol·K
HC <sub>-1</sub>	4.68	0.28	53.78	-160.66	-26.26	-26.26	52.52	-264.32
HC <sub>-2</sub>	-2.48	-7.44	35.45	-128.81	-26.26	-26.26	52.52	-264.32
e-HC <sub>-1</sub>	-69.04	-74.00	-4.80	-207.81	-73.51	-68.26	2.62	-237.73
e-HC <sub>-2</sub>	14.54	9.58	90.75	-243.75	-28.88	-23.63	39.38	-211.34
h <sup>+</sup> -HC <sub>-1</sub>	-84.70	-93.49	-37.77	-167.33	-77.75	-58.17	-8.13	-167.83
h <sup>+</sup> -HC <sub>-2</sub>	-25.74	-30.68	36.74	-202.46	42.47	47.24	108.29	-204.76

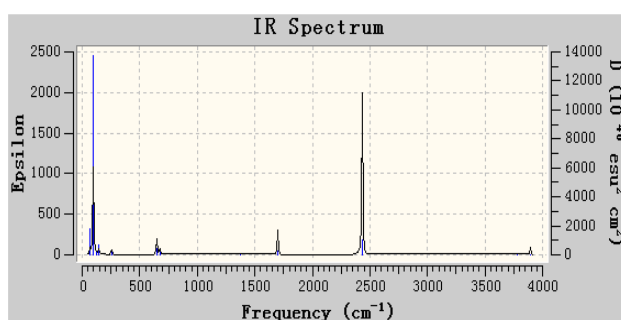
At the computational levels we employed, the skeletal bending vibration of CO<sub>2</sub><sup>•-</sup> was at 711.03 cm<sup>-1</sup>, the symmetrical stretching vibration and the asymmetrical stretching vibration of C=O at 1277.34 cm<sup>-1</sup> and 1621.78 cm<sup>-1</sup> respectively by B3LYP, while the corresponding absorption frequencies of CO<sub>2</sub><sup>•-</sup> by MP2 were at 689.17 cm<sup>-1</sup>, 1232.93 cm<sup>-1</sup> and 1613.98 cm<sup>-1</sup>, respectively.

The infrared absorption spectra of complexes herein became more complicated for the interaction between H<sub>2</sub>O and CO<sub>2</sub> and the effect of photo-induced electrons and holes as shown in Figures 3 and 4. In H<sub>2</sub>O/CO<sub>2-1</sub>, the asymmetrical stretching vibration of O-C≡O at 2342.28 cm<sup>-1</sup> by B3LYP and 2261.42 cm<sup>-1</sup> by MP2, respectively.

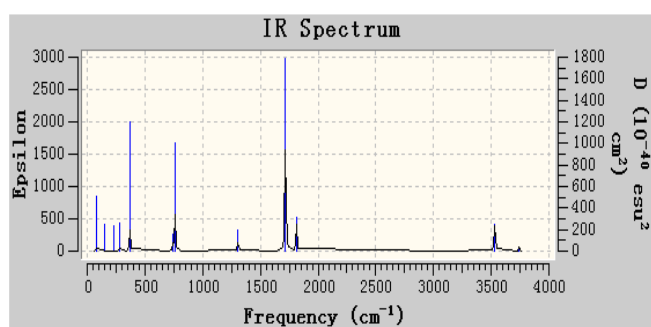
**Figure 3.** IR Spectrum of the complexes at B3LYP/6–311G\* Level (GV 4). (a) H<sub>2</sub>O/CO<sub>2</sub>-1B; (b) H<sub>2</sub>O/CO<sub>2</sub>-2B; (c) e-HC-1B; (d) h<sup>+</sup>-HC-1B; (e) e-HC-2B; (f) h<sup>+</sup>-HC-2B.



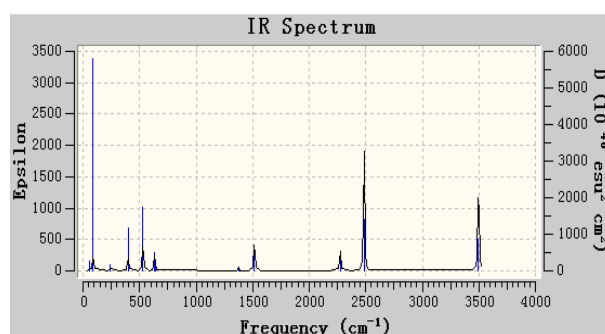
(a) H<sub>2</sub>O/CO<sub>2</sub>-1B



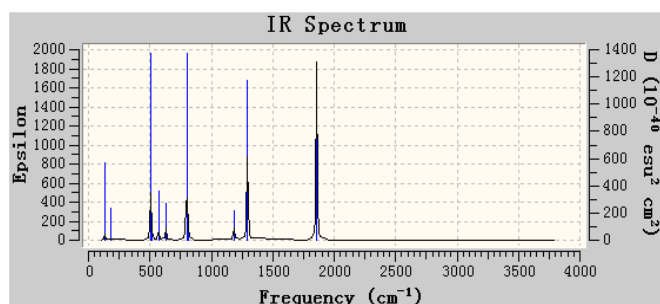
(b) H<sub>2</sub>O/CO<sub>2</sub>-2B



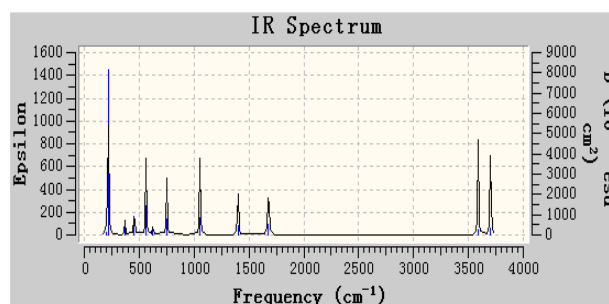
(c) e-HC-1B



(d) h<sup>+</sup>-HC-1B

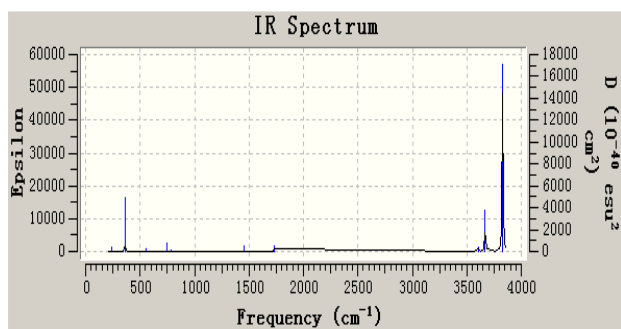


(e) e-HC-2B

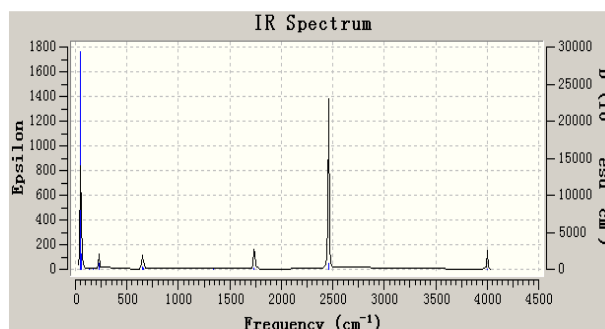


(f) h<sup>+</sup>-HC-2B

**Figure 4.** IR Spectrum of the complexes at MP2/6–311G\* Level (GV 4). (a) h<sup>+</sup>-HC-2M; (b) H<sub>2</sub>O/CO<sub>2</sub>-2M; (c) h<sup>+</sup>-HC-1M; (d) e-HC-1M; (e) H<sub>2</sub>O/CO<sub>2</sub>-1M; (f) e-HC-2M.

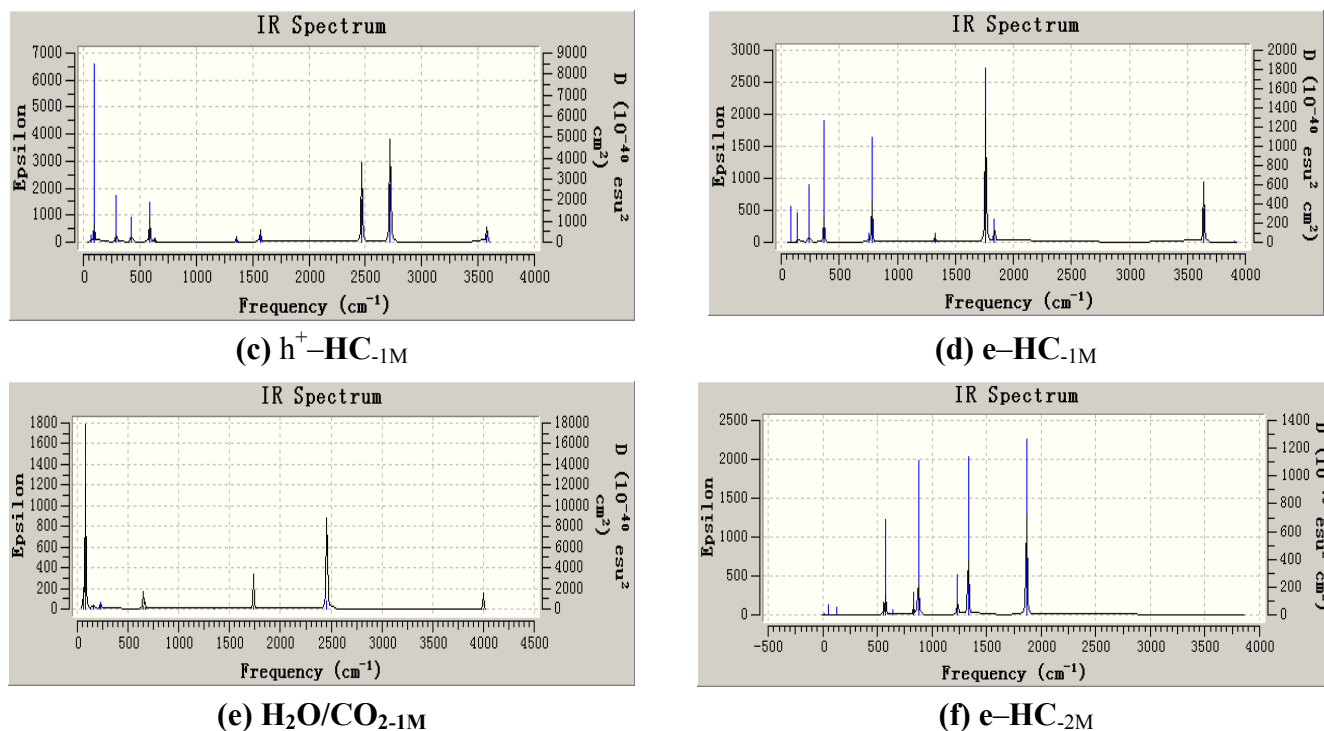


(a) h<sup>+</sup>-HC-2M



(b) H<sub>2</sub>O/CO<sub>2</sub>-2M

Figure 4. Cont.



There was no different infrared absorption between  $H_2O/CO_{2-1}$  and  $H_2O/CO_{2-2}$  by MP2. In  $e-HC_{-1}$ , the stretching vibration of H–O ( $O-H\cdots O=C$ ) was at  $3390.72\text{ cm}^{-1}$  by B3LYP, and the other stretching vibration of H–O at  $3590.40\text{ cm}^{-1}$ , the scissoring rocking vibration of C=O at  $710.40\text{ cm}^{-1}$ , the symmetrical stretching vibration and the asymmetrical stretching vibration of C=O at  $1253.76\text{ cm}^{-1}$  and  $1648.32\text{ cm}^{-1}$ , respectively. By MP2, the infrared absorption frequencies of  $e-HC_{-1}$  were somewhat red shifted. In  $e-HC_{-2}$ , the stretching vibration of  $C\cdots O$  was at  $546.72\text{ cm}^{-1}$  by B3LYP, the symmetrical stretching vibration and the asymmetrical stretching vibration of C=O at  $1242.24\text{ cm}^{-1}$  and  $1782.72\text{ cm}^{-1}$ , respectively. There are many differences of which by MP2, the skeletal rocking vibration at  $513.47\text{ cm}^{-1}$ , the in-plane rocking vibration and the out-of-plane rocking vibration of H–O at  $1137.10\text{ cm}^{-1}$  and  $531.10\text{ cm}^{-1}$ , respectively, the stretching vibration of H–O at  $3525.12\text{ cm}^{-1}$ , the in-plane bending vibration and the out-of-plane bending vibration of C=O at  $765.76\text{ cm}^{-1}$  and  $805.19\text{ cm}^{-1}$ , the symmetrical stretching vibration and the asymmetrical stretching vibration of C=O at  $1225.77\text{ cm}^{-1}$  and  $1716.58\text{ cm}^{-1}$ , the stretching vibration of  $C\cdots O$  at  $587.59\text{ cm}^{-1}$ .

There are some synergistic effects in  $h^+-HC_{-1}$  by B3LYP. The symmetrical stretching vibration of  $O\cdots H-O$  was at  $2182.68\text{ cm}^{-1}$ , the out-of-plane bending vibration and the in-plane bending vibration of  $O-C\equiv O$  at  $603.19\text{ cm}^{-1}$  and  $612.05\text{ cm}^{-1}$ , respectively, the symmetrical stretching vibration of  $O-C\equiv O$  at  $1322.16\text{ cm}^{-1}$ , the synergistic effect of the asymmetrical stretching vibration of  $O\cdots H-O$  and  $O-C\equiv O$  at  $2384.96\text{ cm}^{-1}$ . While by MP2 in  $h^+-HC_{-1}$ , the out-of-plane bending vibration of  $O\cdots H-O$  was at  $538.36\text{ cm}^{-1}$ , the symmetrical stretching vibration and asymmetrical stretching vibration of  $O-C\equiv O$  at  $1356.56\text{ cm}^{-1}$  and  $2275.21\text{ cm}^{-1}$ . The asymmetrical stretching vibration of  $O\cdots H-O$  was at  $2507.93\text{ cm}^{-1}$ , the stretching vibration of H–O at  $3309.60\text{ cm}^{-1}$ . In  $h^+-HC_{-2}$  by B3LYP the in-plane bending vibration of C=O was at  $540.22\text{ cm}^{-1}$ , the stretching vibration of  $C\cdots O$  at  $601.69\text{ cm}^{-1}$ , and the synergistic effect of the asymmetrical stretching vibration of C=O at  $722.74\text{ cm}^{-1}$ , the asymmetrical

stretching vibration of  $\text{H}\cdots\text{O}=\text{C}$  at  $1012.45\text{ cm}^{-1}$ . While by MP2 the stretching vibration of  $\text{C}\cdots\text{O}$  at  $685.57\text{ cm}^{-1}$ , the scissoring rocking vibration of  $\text{C}=\text{O}$  at  $511.11\text{ cm}^{-1}$ , and the symmetrical stretching vibration of  $\text{C}=\text{O}$  at  $1334.48\text{ cm}^{-1}$ . It indicated that both the two calculating method revealed the unreasonable data to  $\text{h}^+-\text{HC}_{-2}$ , therefore the complex was unstable, therefore  $\text{h}^+(\text{H}_2\text{O}/\text{CO}_2)$  had only one stable structure  $\text{h}^+-\text{HC}_{-1}$ .

#### 4. Conclusion

The charge distribution of  $\text{H}_2\text{O}$  and  $\text{CO}_2$  was changed because of the joining of the photo-induced electrons and holes both by MP2 and by B3LYP. The effect from photo-induced electrons and holes in complexes activated  $\text{H}_2\text{O}$  and  $\text{CO}_2$  herein.  $\text{H}_2\text{O}$  has been known to exist as  $-\text{OH}$  group on the surface of catalysts by our experiment and the literature [12].  $\text{H}_2\text{O}$  was activated for the lengthened  $\text{O}-\text{H}$  bond in  $\text{h}^+(\text{H}_2\text{O}/\text{CO}_2)$ . The possible hydrogen bond and  $\text{CO}$  in  $\text{h}^+(\text{H}_2\text{O}/\text{CO}_2)$  indicated that the hole was advantageous during the photoreduction of  $\text{CO}_2$  by  $\text{H}_2\text{O}$ . The IR absorption of  $\text{e}-(\text{H}_2\text{O}/\text{CO}_2)$  and  $\text{h}^+(\text{H}_2\text{O}/\text{CO}_2)$  could not be captured experimentally, and some synergistic effect appeared in IR adsorption spectra which were consistent with the state of complexes and their geometric parameters, therefore the result of calculations revealed useful information for understanding the reaction system.

The results of calculations indicated that the action of photo-induced electrons and holes to  $\text{H}_2\text{O}/\text{CO}_2$  was stronger than the interaction between  $\text{H}_2\text{O}$  and  $\text{CO}_2$ , therefore  $\text{CO}_2$  was activated in  $\text{e}-(\text{H}_2\text{O}/\text{CO}_2)$  and  $\text{h}^+(\text{H}_2\text{O}/\text{CO}_2)$ , the bond length of  $\text{R}_{\text{O}=\text{C}}$  lengthened in  $\text{e}-(\text{H}_2\text{O}/\text{CO}_2)$ , the charge on C and O changed greatly, the density of electron cloud on C strengthened in  $\text{e}-(\text{H}_2\text{O}/\text{CO}_2)$ , and the probability for C to combine with  $-\text{OH}$  or H increased, which might be favorable for forming  $\text{CH}_3\text{OH}$ .

#### Acknowledgement

Financial supports of Natural Science Foundation of Jiangxi Province, China (2007GZH2643) is gratefully acknowledged.

#### References

1. Subrahmanyam, M.; Kaneco, S.; Alonso-Vante N. A Screening for the Photo Reduction of Carbon Dioxide Supported on Metal Oxide Catalysts for C1–C3 Selectivity. *Appl. Catal. B* **1999**, *23*, 169–174.
2. Tseng, I.H.; Chang, W.C.; Wu, J.C.S. Photoreduction of  $\text{CO}_2$  Using Sol-Gel Derived Titania and Titania-Supported Copper Catalysts. *Appl. Catal. B* **2002**, *37*, 37–48.
3. Xie, T.F.; Wang, D.J.; Zhu, L.J.; Li, T.J.; Xu, Y.J. Application of Surface Photovoltage Technique in Photocatalysis Studies on Modified  $\text{TiO}_2$  Photo-catalysts for Photo-reduction of  $\text{CO}_2$ . *Mater. Chem. Phys.* **2001**, *70*, 103–106.
4. Linsebigler, A.L.; Lu, G.J.; Yates, J.T. Photocatalysis on  $\text{TiO}_2$  Surfaces: Principles, Mechanisms, and Selected Results. *Chem. Rev.* **1995**, *95*, 735–758.
5. Sasirekha, N.; Basha, S.; Shanthi, K. Photocatalytic Performance of Ru Doped Anatase Mounted on Silica for Reduction of Carbon Dioxide. *Appl. Catal. B Environ.* **2006**, *62*, 169–180.

6. Yamashita, H.; Fujii, Y.; Ichihashi, Y.; Zhang, S.G.; Ikeue, K.; Park, D.R.; Koyano, K.; Tatsumi, T.; Anpo, M. Selective Formation of CH<sub>3</sub>OH in the Photocatalytic Reduction of CO<sub>2</sub> with H<sub>2</sub>O on Titanium Oxides highly Dispersed within Zeolites and Mesoporous Molecular Sieves. *Catal. Today* **1998**, *45*, 221–227.
7. Zhang, S.G.; Fujii, Y.; Yamashita, K.; Koyano, K.; Tatsumi, T.; Anpo, M. Photocatalytic Reduction of CO<sub>2</sub> with H<sub>2</sub>O on Ti-MCM-41 and Ti-MCM-48 Mesoporous Zeolites at 328 K. *Chem. Lett.* **1997**, *7*, 659–660.
8. Rasko, J.; Solymosi, F. Infrared Spectroscopic Study of the Photoinduced Activation of CO<sub>2</sub> on TiO<sub>2</sub> and Rh/TiO<sub>2</sub> Catalysts. *J. Phys. Chem.* **1994**, *98*, 7147–7152.
9. Lin, W.Y.; Han, H.X.; Frei, H. CO<sub>2</sub> Splitting by H<sub>2</sub>O to CO and O<sub>2</sub> under UV Light in TiMCM-41 Silicate Sieve. *J. Phys. Chem. B* **2004**, *108*, 18269–18273.
10. Anpo, M.; Yamashita, H.; Ikeue, K.; Fujii, Y.; Zhang, S.G.; Ichihashi, Y.; Park, D.R.; Suzuki, Y.; Koyano, K.; Tatsumi, T. Photocatalytic Reduction of CO<sub>2</sub> with H<sub>2</sub>O on Ti-MCM-41 and Ti-MCM-48 Mesoporous Zeolite Catalysts. *Catal. Today* **1998**, *44*, 327–332.
11. Anpo, M.; Yamashita, H.; Ichihashi, Y.; Fujii, Y.; Honda, M. Photocatalytic Reduction of CO<sub>2</sub> with H<sub>2</sub>O on Titanium Oxides Anchored within Micropores of Zeolites: Effects of the Structure of the Active Sites and the Addition of Pt. *J. Phys. Chem. B* **1997**, *101*, 2632–2636.
12. Anpo, M.; Yamashita, H.; Ichihashi, Y.; Ehara, S. Photocatalytic Reduction of CO<sub>2</sub> with H<sub>2</sub>O on Various Titanium Oxide Catalysts of Special Interest. *J. Electroanal. Chem.* **1995**, *396*, 21–26.
13. Xu, Y.J.; Chen, F.M.; Jiang, L.; Zhou, L.D. Photoreduction of CO<sub>2</sub> in the Suspension System of Semiconductor Catalyst TiO<sub>2</sub> Modified by Palladium. *Photogr. Sci. Photochem.* **1999**, *17*, 61–65.
14. Banfield, J.F.; Navrotsky, A. Reviews in Mineralogy and Geochemistry. *Mineral. Soc. Am.* **2001**, *44*, 293–349.
15. Huang, D.; Xiao, Z.D.; Gu, J.H.; Huang, N.P.; Yuan, C.W. TiO<sub>2</sub> Thin-Films Formation on Industrial Glass through Self-Assembly Processing. *Thin Solid Films* **1997**, *305*, 110–115.
16. Li, W.; Shah, S.I.; Hunag, C.P.; Jung, O.; Ni, C. Metallorganic Chemical Vapor Deposition and Characterization of TiO<sub>2</sub> Nanoparticles. *Mater. Sci. Eng. B* **2002**, *96*, 247–253.
17. Luo, D.M.; Chen, C.; Zhang, N.; Hong, S.G.; Wu, H.W.; Liu, Z.H. Characterization and DFT Research of Nd/TiO<sub>2</sub>: Photocatalyst for Synthesis of Methanol from CO<sub>2</sub> and H<sub>2</sub>O. *Z. Phys. Chem.* **2009**, *223*, 1470–1476.
18. Hemminger, J.C.; Carr, R.; Somorjai, G.A. The Photoassisted Reaction of Gaseous Water and Carbon Dioxide Adsorbed on the SrTiO<sub>3</sub> (111) Crystal Face to form Methane. *Chem. Phys. Lett.* **1978**, *57*, 100–104.
19. Ikeue, K.; Nozaki, S.; Ogawa, M.; Anpo, M. Characterization of Self-standing Ti-containing Porous Silica Thin Films and Their Reactivity for the Photocatalytic Reduction of CO<sub>2</sub> with H<sub>2</sub>O. *Catal. Today* **2002**, *74*, 241–248.
20. Inokuchi, Y.; Kobayashi, Y.; Muraoka, A.; Nagata, T.; Ebata, T. Structures of water-CO<sub>2</sub> and methanol-CO<sub>2</sub> cluster ions: [H<sub>2</sub>O•(CO<sub>2</sub>)<sub>n</sub>]<sup>+</sup> and [CH<sub>3</sub>OH•(CO<sub>2</sub>)<sub>n</sub>]<sup>+</sup> (n = 1–7). *J. Chem. Phys.* **2009**, *130*, 1–12.
21. Hohenberg, P.; Kohn, W. Inhomogeneous Electron Gas. *Phys. Rev. B* **1964**, *136*, B864–B871.
22. Kohn, W.; Sham, L.J. Self-Consistent Equations Including Exchange and Correlation Effects. *Phys. Rev.* **1965**, *140*, A1133–A1138.

23. Gerratt, J.; Mills, I.M. Force Constants and Dipole-Moment Derivatives of Molecules from Perturbed Hartree–Fock Calculations. *J. Chem. Phys.* **1968**, *49*, 1719–1729.
24. Pulay, P. Second and Third Derivatives of Variational Energy Expressions-application to Multi-configurational Self-consistent Field Wave-functions. *J. Chem. Phys.* **1983**, *78*, 5043–5051.
25. Vosko, S.H.; Wilk, L.; Nusair, M. Accurate Spin-dependent Electron Liquid Correlation Energies for Local Spin Density Calculations: A Critical Analysis. *Can. J. Phys.* **1980**, *58*, 1200–1211.
26. Lee, C.T.; Yang, W.T.; Parr, R.G. Development of the Colle-Salvetti Correlation-energy Formula into a Functional of the Electron Density. *Phys. Rev. B* **1988**, *37*, 785–789.
27. Becke, A.D. Density-functional Thermochemistry. III. The Role of Exact Exchange. *J. Chem. Phys.* **1993**, *98*, 5648–5652.
28. Becke, A.D. Density-functional Exchange-Energy Approximation with Correct Asymptotic Behaviour. *Phys. Rev. A* **1988**, *38*, 3098–3100.
29. McLean, A.D.; Chandler, G.S. Contracted Gaussian-basis Sets for Molecular Calculations. 1. 2nd Row Atoms,  $Z = 11$ –18. *J. Chem. Phys.* **1980**, *72*, 5639–5648.
30. Møller, C.; Plesset, M.S. Note on an Approximation Treatment for Many-electron Systems. *Phys. Rev.* **1934**, *46*, 618–622.
31. Krishnan, R.; Binkley, J.S.; Seeger, R.; Pople, J.A. Self-Consistent Molecular Orbital Methods. 20. Basis set for Correlated Wave-functions. *J. Chem. Phys.* **1980**, *72*, 650–654.
32. Frisch, M.J. *Gaussian 94*, Revision E.2; Gaussian: Pittsburgh, PA, USA, 1995.
33. Frisch, M.J.; Trucks, G.W.; Schlegel, H.B.; Scuseria, G.E.; Robb, M.A.; Cheeseman, J.R.; Montgomery, J.A., Jr.; Vreven, T.; Kudin, K.N.; Burant, J.C., *et al.* *Gaussian 03*, Revision E.01; Gaussian Inc.: Wallingford, CT, USA, 2004.
34. Li, Z.; Wang, L.; Ran, H.; Xie, D.; Blinov, N.; Roy, P.N.; Guo, H. Path integral Monte Carlo study of CO<sub>2</sub> solvation in 4He clusters. *J. Chem. Phys.* **2008**, *128*, 224513:1–224513:7.
35. DelBene, J.E. Ab initio Molecular Orbital Study of the Structures and Energies of Neutral and Charged Bimolecular Complexes of Water with the Hydrides AH<sub>n</sub> (A = nitrogen, oxygen, fluorine, phosphorus, sulfur, and chlorine). *J. Phys. Chem.* **1988**, *92*, 2874–2880.
36. Binkley, J.S.; Pople, J.A. Møller-Plesset Theory for Atomic Ground State Energies. *Int. J. Quantum Chem.* **1975**, *9*, 229–236.
37. Feller, D. Application of Systematic Sequences of Wave-functions to the Water Dimer. *J. Chem. Phys.* **1992**, *96*, 6104–6114.
38. Kim, K.S.; Mhin, B.J.; Choi, U.S.; Lee, K. Ab-initio Studies of the Water Dimer using large Basis set: The Structure and Thermodynamics Energies. *J. Chem. Phys.* **1992**, *97*, 6649–6662.
39. Szalewicz, K.; Cole, S.J.; Kolos, W.; Bartlett, R.J. A Theoretical Study of the Water. Dimer Interaction. *J. Chem. Phys.* **1988**, *89*, 3662–3673.
40. Frisch, M.J.; DelBene, J.E.; Binkley, J.S.; Schaefer, H.F., III. Retical Studies of the Hydrogen-bonded Complexes (H<sub>2</sub>O)<sub>2</sub>, (H<sub>2</sub>O)<sub>2</sub>H<sup>+</sup>, (HF)<sub>2</sub>, (HF)<sub>2</sub>H<sup>+</sup>, F<sub>2</sub>H<sup>-</sup>, and (NH<sub>3</sub>)<sub>2</sub>. *J. Chem. Phys.* **1986**, *48*, 2279–2289.